Enhancing capillary trapping effectiveness through proper time scheduling of injection of supercritical CO_2 in heterogeneous formations

Ana González-Nicolás

Luca Trevisan

Tissa H. Illangasekare

Abdullah Cihan

Jens T. Birkholzer
First published: 23 November 2016
https://doi.org/10.1002/ghg.1646
UC-eLinks

Abstract

The impact of geologic heterogeneity on capillary trapping of supercritical CO_2 ($scCO_2$) has been recognized and appraised through laboratory experimentation and modeling. However, how different injection strategies can be optimized to improve capillary trapping has not received adequate attention. We present a study based on stochastic analysis to show the impact of injection scheduling on capillary trapping of $scCO_2$ in heterogeneous geological formations. Improvement of trapping efficiency consists of maximizing the trapped volume within a predefined secure zone of the storage formation with the goal of avoiding plume intersection with potential leakage pathways. Using knowledge acquired from physical experiments in intermediate-scale tanks with controlled heterogeneity, we conduct numerical simulations following a stochastic approach to extend the observed outcomes to a series of equally probable permeability scenarios. Our simulations involve the same combination of surrogate fluids that are used in the experiments to mimic viscosity and density contrasts between $scCO_2$ and brine. To account for uncertainty of formation heterogeneity, several permeability fields with three different variances and two horizontal correlation lengths are generated. The same volume of $scCO_2$ is emplaced using four different modes of injection scheduling. Results suggest that injection strategies aimed at enhancing capillary trapping of $scCO_2$ and increasing the probability of constraining the plume within a secure zone are strictly related to the specific heterogeneity of the reservoir. This preliminary theoretical finding suggests the potential for maximizing secure capillary trapping through the proper selection of injection schedule to fit the formation heterogeneity.

Introduction

In addition to spatial continuity of a sealing caprock, the influence of permeability heterogeneity on trapping of supercritical CO_2 ($scCO_2$) during injection and storage operations is considered

crucial to determine viability of geological repositories. Several field experiments and numerical modeling studies suggest that considerable amounts of CO_2 can be stored in sedimentary formations exhibiting variable degrees of intra-reservoir heterogeneity. Some examples of modeling studies that included simulations of $scCO_2$ injection into stochastically generated heterogeneous formations are presented as follows. Doughty and Pruess[1]highlighted the impact of end-point relative permeability on CO_2 plume spreading, showing an increase in CO_2 capillary trapping for high residual gas saturations. At the Frio pilot site in Texas, Hovorka *et al*.[2] considered the effect of stratigraphic and structural heterogeneity on CO_2 storage, introducing concepts such as sequestration capacity and effectiveness. Through a stochastic analysis of geostatistical parameters describing six permeability distributions, Lengler *et al*.[3] studied the impact of heterogeneity on the injectivity and gas saturation at the Ketzin test site in Germany. They concluded that displacement efficiency and storage capacity increase with the tortuosity of the migration path caused by heterogeneity, whereas the average injectivity of the formation decreases. An analogous observation was brought by Flett *et al*.,[4] who investigated the effects of net-to-gross sand ratio on the migration and trapping of $scCO_2$ in the Gorgon field in North West Australia. Although they disregarded the effect of correlation length of the shale facies, they showed how the presence of shale is directly correlated with the lateral spreading of the CO_2 plume and inversely correlated with the vertical migration. Similarly, Green and Ennis-King[5] focused on the effects of vertical heterogeneity on the CO_2 displacement. They concluded that a buoyant CO_2 plume moving across a heterogeneous formation has a lower breakthrough time than in a homogeneous formation with equivalent permeability. By correlating $P_c(S)$ relationship with permeability for all grid-blocks of their modeling domain, Saadatpoor *et al*.[6] concluded that the intrinsic heterogeneity becomes relevant when capillary trapping occurs in conjunction with low-permeability facies during vertical advancement of the plume. For this reason, differences in the capillary entry pressure can hinder the buoyancy-driven flow of $scCO_2$ producing local accumulations at saturations above residual underneath low permeable regions. Han *et al*.[7]showed that increasing the anisotropy ratio between horizontal and vertical permeability favors the trapping of residual CO_2. They also showed that presence of low-permeability thin layers increases the residual CO_2 trapping. Recently, Gershenzon *et al*.[8] showed how small-scale heterogeneities within larger-scale features are critical to understand trapping processes in CO_2 reservoirs that present sedimentary architecture.

Several laboratory studies investigated the influence of intra-reservoir heterogeneity on buoyant fluid displacement and capillary trapping in the context of multiphase flow of CO_2 and brine.[9-13] Krevor *et al*.[10] conducted core flooding experiments to study the variability of CO_2trapping

due to capillary heterogeneity. They observed that CO_2 accumulated at barriers of low-permeability layers leads to locally trapped CO_2 saturations higher than residually trapped values. Trevisan *et al.*[13] used surrogate fluids and x-ray attenuation analysis to study the ability of sequential injections of $scCO_2$ to enhance the contact between plume and resident fluid, as well as the volume of non-wetting phase trapped by capillary forces. By conducting intermediate-scale experiments in a controlled heterogeneous permeability field and comparing plume migration and ultimate trapping with an ideally homogenous scenario, they observed how larger plume footprints and longer residence times are attained with sequential injections and heterogeneous permeability fields, respectively. More recently, the influence of drainage and imbibition cycles on residual trapping has been studied through experiments realized at pore-scale.[14] Results of this study suggest that residual trapping of $scCO_2$ is increased when several cycles of drainage and imbibition are applied.

Despite the efforts to understand the impact of heterogeneity on increasing $scCO_2$ trapping, the potential use of injection scheduling to enhance the $scCO_2$ trapped by capillary forces in heterogeneous formations has not yet received adequate attention. Common challenges addressed by numerical studies include how to maximize storage capacity and displacement efficiency by optimizing well location and CO_2 injection rates,[15] as well as injection and extraction of brine,[16] and others the water-alternating-gas technique.[17, 18] Shamshiri and Jafarpour[15] investigated the optimization of CO_2 storage in a heterogeneous aquifer by applying two methods: CO_2 flooding sweep efficiency and total stored gas. The latter method produces greater storages controlling the injection rate allocations within several injection wells. Cameron and Durlofsky[16] studied the well-placement and CO_2 injection rates, as well as brine injection in a heterogeneous medium to maximize dissolution and residual trapping. They observed that brine injection decreases the mobile fraction of CO_2. However, both the Shamshiri and Jafarpour study[15] and the Cameron and Durlofsky study[16] neglect capillary pressure effects.

In other applications of multiphase fluid trapping in heterogeneous porous media has been studied in relevance to subsurface remediation and enhanced oil recovery. For instance, Illangasekare *et al.*[19] highlight the influence of the injection rate on the degree of dense organic contaminants spreading in heterogeneous aquifers. The contaminant travels further horizontally when a larger spill rate of the contaminant is implemented.

Trevisan *et al.*[20] carried out a set of immiscible displacement experiments in laboratory test systems with the goal of demonstrating how the formation heterogeneity affects plume migration and ultimately contributing to trapping enhancement. They used a combination of surrogate fluids for $scCO_2$ and brine to conduct experiments in intermediate scale under ambient laboratory

conditions. The effect of heterogeneity on overall capillary trapping capacity was studied by comparing idealized homogeneous base case with a heterogeneous scenario. Moreover, enhancement of trapping efficiency was observed when implementing a placement strategy consisting of two injection events followed by as many post-injection periods. The experiments showed larger amounts of non-wetting phase (NWP) could be stored after a second injection event; however, larger emplaced volumes also increased likelihood in plume escaping the control area, suggesting the need to investigate this phenomenon with a stochastic approach.

The goal of the work presented in this paper is to extend Trevisan *et al*.[20] experimental study and to investigate whether injection scheduling significantly affects the capillary trapping of $scCO_2$ in naturally heterogeneous geologic formations. We apply four different injection strategies composed of cycles of injection pulse and relaxation time (or post-injection) to assess the capillary trapping performance of four ensembles of permeability distributions. In practice, several time-distributed injection pulses can be performed using multiple injection wells. Using the heterogeneous configuration applied in experiment documented in Trevisan *et al*.[20] as a basis, a stochastic analysis was carried out to investigate the impact of sequential injection on enhancing $scCO_2$ storage in synthetic reservoirs with variable statistical properties, such as variance and horizontal correlation length. The CO_2 injection strategies were applied to four ensembles of 500 realizations. Realizations within each ensemble share the same geostatistical parameters defining the spatially distributed two-dimensional (2D) permeability fields.

A key goal in successful geological carbon sequestration is to use the formation most effectively to secure the storage through stable trapping of the injected $scCO_2$. It is expected that deep formations selected for geological carbon sequestration might contain potential pathway for $scCO_2$ to leak. Potential pathways might be abandoned wells, faults and fractures, and permeable areas of the sealing formation.[21] Here we define a successful simulation as a simulation that contains the $scCO_2$ plume in a predefined secure zone as constrained by the locations of the potential leakage pathways. Also, the no interaction with on-going oil/gas or other injection/extraction projects could be considered as constraints of the secure zone. Analyses of the spatial moments of the $scCO_2$ saturation distribution were used to quantitatively assess the effectiveness of capillary trapping. This paper is organized as follows. Next section describes the methodology used and the numerical experiment. Then results of the stochastic analysis are presented and discussed. Finally, the main conclusions of this study are summarized.

Methods and problem set-up

Numerical model

The stochastic analysis was performed using an in-house two-phase flow simulator that has the capability to simulate the non-wetting fluid migration and capillary trapping in heterogeneous systems. Two partial differential equations based on pressure-saturation are solved with the finite volume method using an implicit Euler scheme for time discretization. The resulting system of coupled non-linear equations is solved using the Newton-Raphson method. At each Newton-Raphson iteration, a generalized preconditioned minimum residual algorithm is applied. The numerical model is based on the mass conservation equation (Eqn 1) and Darcy equation (Eqn 2):

$$\frac{\partial\left(\varphi\rho_\gamma S_\gamma\right)}{\partial t} = -\nabla\cdot\left(\rho_\gamma \boldsymbol{u}_\gamma\right) + q_\gamma \quad (1)$$

$$\boldsymbol{u}_\gamma = -\frac{\boldsymbol{k}k_{r\gamma}}{\mu_\gamma}\cdot\left(\nabla P_\gamma + \rho_\gamma g\nabla z\right) \quad (2)$$

where φ is the porosity, ρ is the density, S is the saturation, u is the Darcy velocity, q is the source/sink term, and t represents time. The subscript γ represents the phase: either the non-wetting (NWP) or the wetting (WP) phase. Variables k, k_r, and μ are the intrinsic permeability, relative permeability and viscosity, respectively. Fluid phase pressure is defined as P and g is the acceleration due to gravity. The two fluid phases are assumed to be incompressible and fully immiscible. The two-phase flow simulator does not consider hysteresis. The two-phase flow parameters are based on the van Genuchten capillary pressure–saturation constitutive model:[22]

$$S_w\ (P_c) = \left[S_e\,(P_c) \times \left(S_W^{max} - S_W^{irr}\right)\right] + S_W^{irr} \quad (3)$$

where the effective saturation S_e is a function of the wetting phase saturation S_W $(S_e = (S_W - S_W^{irr})/(1 - S_W^{irr}))$ and the maximum and irreducible wetting phase saturation, S_W^{max} and S_W^{irr}, respectively. The effective saturation is related to the capillary pressure defined through:

$$S_e\,(P_c) = \left[1 + (\alpha P_c)^n\right]^{-m} \quad (4)$$

P_c is the capillary pressure defined by the difference of pressures between NWP and WP. n, m, and α represent the fitting parameters of the van Genuchten model. In this study the van Genuchten-Mualem relative permeability model[23] was used:

$$k_{r,W} = S_e^{L_W}\left[1 - \left(1 - S_e^{1/m}\right)^m\right]^2 \quad (5)$$

$$k_{r,NW} = \left(1 - S_{e,NW}\right)^{L_{NW}}\left(1 - S_{e,NW}^{\frac{1}{m}}\right)^{2m}$$

$$\text{if}\quad S_{NW} \geq S_{r,NW}$$

$$k_{r,NW} = 0\ \text{if}\quad S_{NW} < S_{r,NW} \quad (6)$$

where $k_{r,W}$ and $k_{r,NW}$ correspond to the relative permeability of the WP and NWP, respectively, L_W and L_{NW} are experimentally fitted parameters of the van Genuchten-Mualem model related to tortuosity of the pore space, and $S_{e,NW} = (S_W - S_W^{irr})/(1 - S_W^{irr} - S_{r,NW})$. $S_{r,NW}$ is the residual saturation of the NWP.

Simulation domain and set-up

The numerical domain setup reflects the geometry of the 244 × 5 × 80.8 cm^3 tank experiments described in Trevisan *et al*.[20] Heterogeneity of the packing is configured with a natural-logarithmic distribution of the permeability (ln*k*) discretized in six categories, each representing a sieve size of Granusil silica sand. The permeability field has a mean ln*k* (*k* in m^2) of -24.1 and a variance of 1.69. Table 1 lists the physical properties of the six sand types including permeability and average porosity (φ_{avg}). A long horizontal (λ_x = 33.3 cm) and short vertical (λ_z = 1.3 cm) correlation lengths are used to create a longer spread of the plume horizontally and delay the vertical migration towards the caprock.

Table 1. Physical properties of silica sands.[24]

Sand	Sieve size	*k* (m^2)	ln*k*	ϕ_{avg} (-)
1	#16	5.62×10^{-10}	−21.3	0.40
2	#20	2.14×10^{-10}	−22.3	0.41
3	#30	1.23×10^{-10}	−22.8	0.43
4	#50	3.37×10^{-11}	−24.1	0.40
5	#70	1.43×10^{-11}	−25.0	0.44
6	#110	5.21×10^{-12}	−26.0	0.38

The surrogate fluids for $scCO_2$ into a saline formation were Soltrol 220 (dyed with Sudan IV and doped with 10% *w/w* Iodoheptane) as the NWP and a glycerol-water mixture (80:20) as the WP. A total NWP volume of 2 L was injected in the experimental aquifer, which was distributed during two injection events. Using the setting of the tank to define the test domain, the sands were distributed in a 2D grid of 122 gridlines in the horizontal direction and 25 gridlines in the vertical direction with uniform grid-block dimensions of 2 cm by 2 cm. The 122 gridlines in the horizontal direction included the two vertical boundaries of the test domain. The configuration of the layers followed a dipping angle of 3°.

Figure 1 shows dimensions of the flow domain (244 cm × 5 cm × 50 cm), the heterogeneous sand packing configuration and digital images of immiscible fluid displacement captured for three different times. Figure 1(a) displays the plume distribution at the end of the first injection (at 27.3 h and 1 L of Soltrol 220 injected), whereas Fig. 1(b) captures the plume at the end of the second injection (at 293.42 h and 2 L of Soltrol 220 injected). The last panel, Fig. 1(c), shows the final distribution of the plume at time 2400 h.

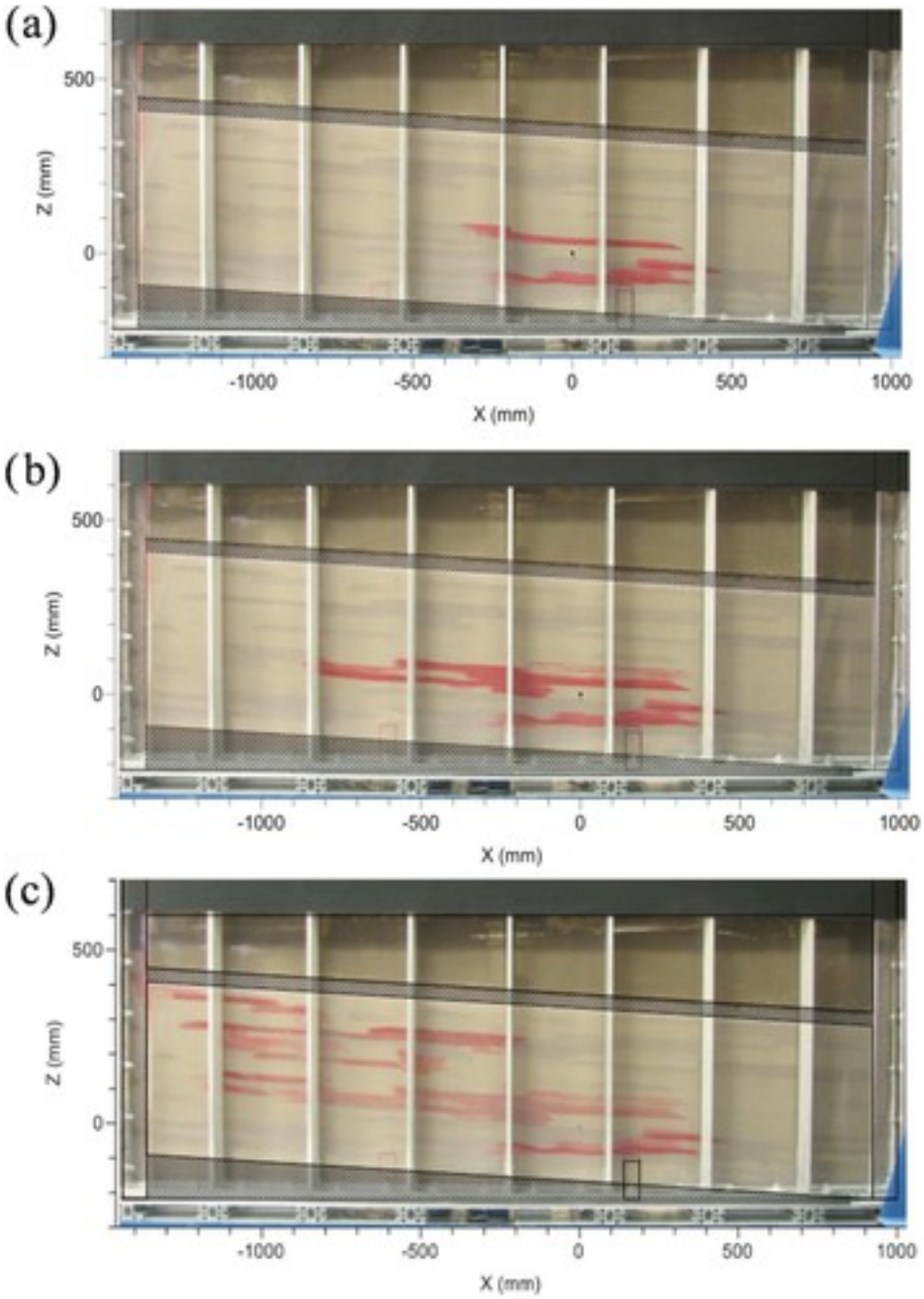

Figure 1

Open in figure viewerPowerPoint

Plume distribution across the heterogeneous aquifer: (a) End of first injection (27.3 h), (b) End of second injection (293.42 h), and (c) Final distribution (2400 h). Black rectangle shows location of the injection well.25

Caption

In the numerical model simulations, the same total volume of 2 L of NWP was injected into the formation based on several injection strategies. Each injection strategy has a specific distribution of injecting pulses within a total time of 24.16 days. Table 2 describes the four injection

strategies I to IV. The number of cycles in Table 2 refers to the number of times that the injection period and relaxation time are repeated. Thus, the injection strategy II, which includes two cycles, is constituted by (injection cycle + relaxation time) + (injection + relaxation time) applying the injection rates and lengths described in Table 2.

Table 2. Injection strategies applied to the four stochastic storage scenarios simulations 1 to 4.

	Injection cycle			
Injection strategy	**Rate (L/d)**	**Duration (d)**	**Time interval between injection cycles (d)**	**Number of cycles***
I	1.04	1.92	–	1
II	1.04	0.96	11.12	2
III	1.04	0.64	7.41	3
IV	1.04	0.48	5.56	4
A	1.33	0.75	0.42	2
B	2.00	0.50	0.92	2
C	1.33	1.50	–	1

- *The number of cycles refers to the number of times that the injection cycles and relaxation time are repeated.

A 2D vertical cross-sectional model domain with the dimensions and dipping angle of the experimental setup in Fig. 1 was used. A discretization of 2 cm m × 5 cm × 2 cm was applied. Constant pressure was applied to the lateral boundaries to constrain a steady-state WP flow corresponding to a horizontal hydraulic gradient of 0.044. No-flow conditions were assigned to the top and bottom layers of the aquifer. Constant saturation of the NWP is applied to the left and right boundaries of the tank. Thus, the NWP can freely leave the tank but not its reentrance, avoiding the generation of secondary plumes into the reservoir. The injection of the $scCO_2$ occurred through one injection well located at the bottom of the aquifer at x = 0.13 m and x = 0.17 m and z = 0.04 m and z = 0.06 m. Table 3 includes the fluid properties used in this study. Data to determine the parameters of the constitutive models defining the relations of capillary pressure and saturation (Eqn 3) and relative permeability (Eqns 5 and 6) for the primary drainage of each sand were generated by Vargas-Johnson26 and given in Table 4.

Table 3. Fluid properties of the NWP and WP.

Fluid property (units)	Value
ρ_{NW} (kg/m^3)	860
ρ_W (kg/m^3)	1210
μ_{NW} (Pa· s)	4.9×10^{-3}
μ_W (Pa· s)	6.1×10^{-2}

Table 4. Van-Genuchten model fitting parameters for the silica sands.

		Sand					
	Parameter	**1**	**2**	**3**	**4**	**5**	**6**
	S_W^{max}	0.75	0.78	0.78	0.72	0.85	0.85
	$S_{NW,r}^{max}$	0.25	0.22	0.22	0.28	0.15	0.15
	S_W^{irr}	0.08	0.07	0.07	0.07	0.006	0.1
Primary drainage	α	20	15	15	10	9.86	6.04
	n	5	5	5	6	10	9.03
	m	0.80	0.80	0.80	0.64	0.90	0.89

To generate the spatial distributions of permeability based on the geostatistical parameters used in the experiments by Trevisan *et al.*,[20] a sequential indicator simulation algorithm of the geostatistical library GSLIB[27] coupled to the SGeMS[28] open source software was used. The spatial distributions of permeability were generated with a fine 2D regular grid of 0.02 m × 0.02 m. Each ensemble of permeability distributions is referred to as simulation 1 through 4 and is composed by 500 equiprobable realizations. Different natural-logarithmic variances and correlation lengths are applied to each spatial distribution. The correlation lengths follow an exponential variogram. The geostatistics parameters of each spatial distribution including mean, variances, and correlation lengths are presented in Table 5. Note that simulation 2 in Table 5 is based on the experimental scenarios reported in Trevisan *et al.*[20] Figure 2 presents the probability distribution function of each sand category from Table 1 for the three variances applied to simulations 1 to 4 and one example of material distribution for simulations 1 to 4.

Table 5. Geostatistical parameters used for populating the flow domain grid with different degrees of spatial variation of permeability.

Simulation	ln*k* mean	ln*k* variance	λ_x(cm)	λ_z (cm)	Number of realizations	Injection strategy
1	−24.1	1.00	33.3	1.3	500	I, IV
2*	−24.1	1.69	33.3	1.3	500	I, II, III, IV
3	−24.1	2.89	33.3	1.3	500	I, IV
4	−24.1	1.69	6.7	1.3	500	I, IV

- *Spatial distribution implemented in the experimental case20

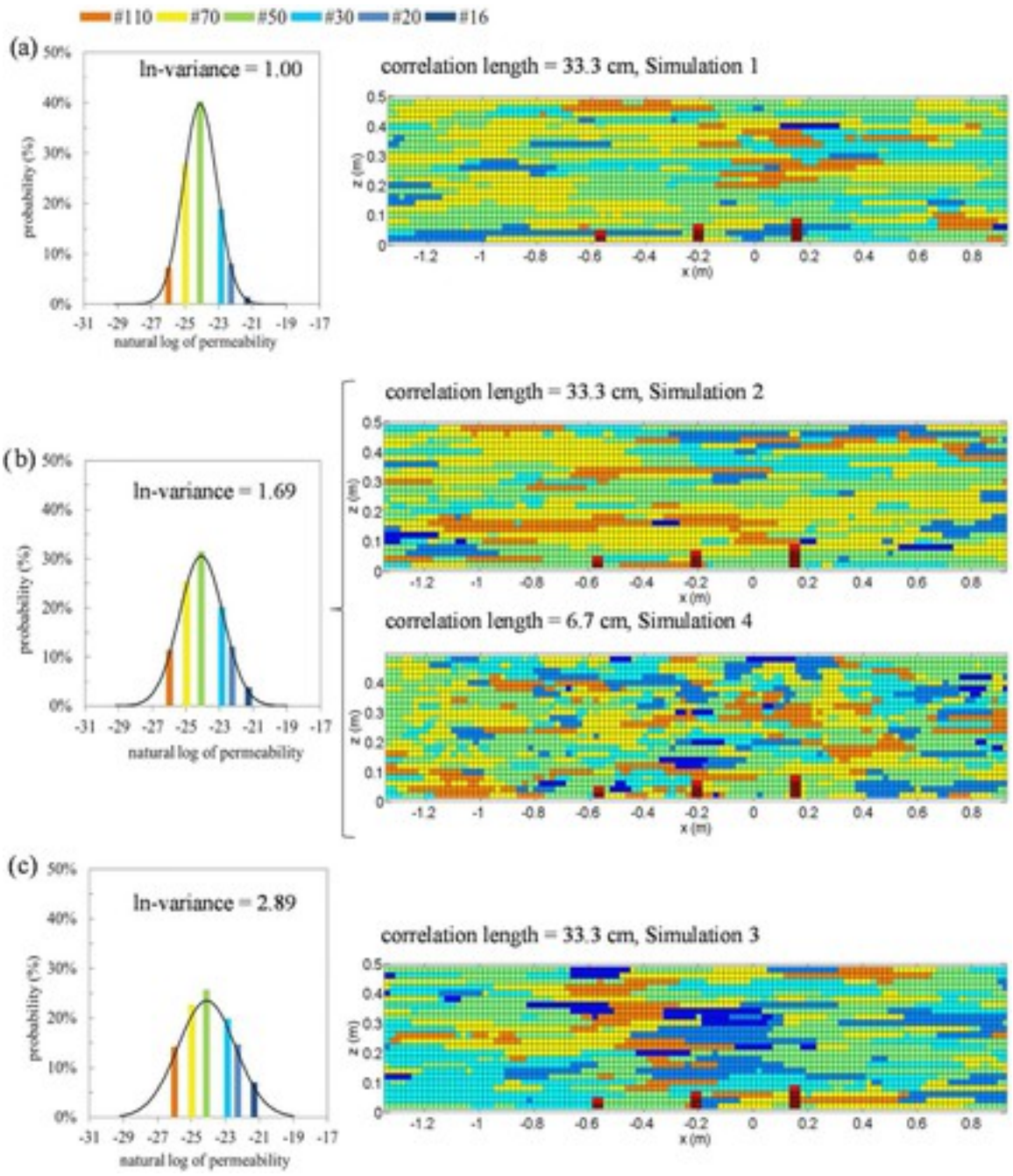

Figure 2

[Open in figure viewerPowerPoint]

Left column: Target histograms of the natural log of intrinsic permeability (in m^2) with ln*k* mean -24.1 (#50 sand) and (a) ln*k* variance = 1.00 (simulation 1), (b) ln*k* variance = 1.69 (simulations 2 and 4), and (c) ln*k* variance = 2.89 (simulation 3). Right column: material distributions within the boundaries of one realization for each target histogram.

Caption

Spatial moment analysis and plume-scale effective trapping saturation

For this study, we define a *secure zone* as the area delimited by the tank boundaries and a *successful realization* as a realization of the permeability field that contains the total NWP volume injected in the secure zone. To evaluate the lateral and vertical migration and spread of the plume spatial moment evolution throughout the simulations were analyzed. The zerothmoment M_{00} is a measure of the total NWP volume in the tank. The first and second spatial moments provide information about the distribution (or location) and spreading of the plume, respectively. These moments are defined as (adapted for saturation from Freyberg[29]):

$$M_{ik}(t) = \Delta y \iint \varphi(x,z)\, S_{NW}(x,z,t) x^i z^k dx dz \quad (7)$$

where $M_{ik}(t)$ is the ik^{th} moment of the NW volume distribution; i and k denote the x and $z$directions and are equal to 0, 1, or 2 to refer the zeroth, first, and second moment, respectively; φ and S_{NW} are the porosity and NW saturation at location (x, z). Δy is the depth of the tank (5 cm). Note that the saturation also depends on time t. The center of the NWP volume (x_c, z_c) is defined by the first and zeroth moment:

$$x_c = M_{10}/M_{00}$$
$$z_c = M_{01}/M_{00} \quad (8)$$

The lateral spreading of the NWP volume is represented by:

$$\sigma_{xx} = M_{20}/M_{00} - x_c^2$$
$$\sigma_{zz} = M_{02}/M_{00} - z_c^2 \quad (9)$$

Results and discussion

Four stochastic simulations referred to as simulation 1 through 4 were carried out applying the permeabilities spatial distributions and sequential injections described in Tables 5 and 2, respectively. A total volume of 2 L was introduced in each simulation and results are presented between 24.16 days and the end of the simulation at 100 days. The NWP plume reaches a more or less steady state during this interval of time. In the experimental study[20] for the heterogeneous case and two injections periods, the steady state was observed after 80 days, while for the homogeneous case it was at 24 days.

Table 6 lists the number of realizations (for each simulation) in which the total volume of NWP (2 L) remained in the secure zone at t = 100 days. Note that the number of realizations (or cases) in which the totality of the NWP volume is trapped in the secure zone increases when fewer of injection pulses are applied (e.g. injection strategy I versus IV) and when the degree of heterogeneity increases (e.g. simulation 4 versus simulation 2). However, for the specific simulations 1 to 3 of this study, the number of successful realizations increases with a lower

variance of the permeability. Simulations 1 to 3 present a long correlation length, which can favor the escape of the plume from the secure zone if the plume of $scCO_2$ finds very permeable zones leading to the boundaries of the tank. Therefore, simulation 3 with a higher variance of the permeability (high presence of zones with very low and high permeability) shows the lowest number successful realizations in Table 6.

Table 6. Number of successful realizations in which $scCO_2$ plume is trapped in its totality (2 L) in the secure zone at t = 100 days.

	Injection strategy			
Simulation	**I**	**II**	**III**	**IV**
1	118	—	—	93
2	88	86	69	60
3	42	—	—	37
4	310	—	—	274

Simulation 2-I, with only one injection and one relaxation cycle, has a total of 88 realizations (out of 500) in which the NWP remains within the secure zone. The number of cases for which the plume remained in the secure zone for simulations 2-II, 2-III, and 2-IV are 86, 69, and 60, respectively. Decreasing the number of injection cycles from four to one (injection strategy IV and I, respectively) slightly increases the containment of the plume in the secure zone by 5.6%. The fact that the injection strategy I produces better outcome in containing the plume in the desired area is also observable for simulations 1, 3, and 4. Table 7 shows the percentage of NWP that has leaked out of the secure zone at t = 100 days. Note that the total volume injected for one simulation is 1000 L (500 realizations × 2 L). Leakages of NWP for injection strategy IV are slightly greater than leakages of NWP for injection strategy I for each ensemble of simulations.

Table 7. Leakage of $scCO_2$ (%) from the secure zone at t = 100 days.

	Injection strategy			
Simulation	**I**	**II**	**III**	**IV**
1	9.1	—	—	12.8
2	13.6	14.7	16.3	17.6
3	19.3	—	—	23.5
4	3.0	—	—	4.5

The impact of the variance on the NWP containment is reflected by results of simulations 1, 2, and 3. Simulations 1-I and 1-IV, which were generated with a lower permeability variance (Table 5), produce more cases in which the NWP is trapped in the secure zone in comparison to simulations 2-I and 2-IV, and 3-I and 3-IV. Anisotropy of permeability in the vertical direction plays an important role. Low permeable areas hinder the vertical spread of the NWP; thus, the plume is forced to travel horizontally through areas with higher permeability. High permeability variance, such as in simulation 3, implies that there is more probability for categories with lower and higher permeability than the mean permeability; therefore, the plume can spread more easily laterally than vertically. Simulations 4-I and 4-IV with the lowest correlation length (Table 5) present the greatest number of realizations in which the NWP is contained in the secure zone. In these simulations, the spatial distribution of the six categories of sands present shorter preferential path that limits the probability of the plume to reach the tank boundary. On the other hand, simulation 2, which is created with same variance as simulation 4, produces fewer cases in which the NWP is contained in the tank boundaries. Greater λ_x of the sands categories enhance the escape of the NWP through preferential pathways of high permeability; therefore, NWP can reach further areas of the formation by spreading horizontally. These results agree with Han *et al.*7 and Lengler *et al.*3

Consistently, for all four spatial distributions of permeabilities (simulations 1 to 4), injection strategies involving less cycles of injection produce a higher saturation of the NWP plume. Figure 3 shows the average NWP saturation value for simulations 1 to 4 and injection strategies I and IV. Injection strategy I presents distributions of the NWP with slightly higher saturation independently of the heterogeneity of the sand distributions or variance (simulations 1 to 3). Only simulation 4 presents a slightly higher distribution of the NWP around the injection well for injection strategy IV. Note that simulation 4 generated with a lower correlation length presents a higher distribution of the plume vertically reaching the top boundary in Fig. 3; whereas NWP plumes of simulations 1, 2, and 3 (with greater λ_x) do not reach the top of the formation in Fig. 3, since NWP seems to be displaced more horizontally.

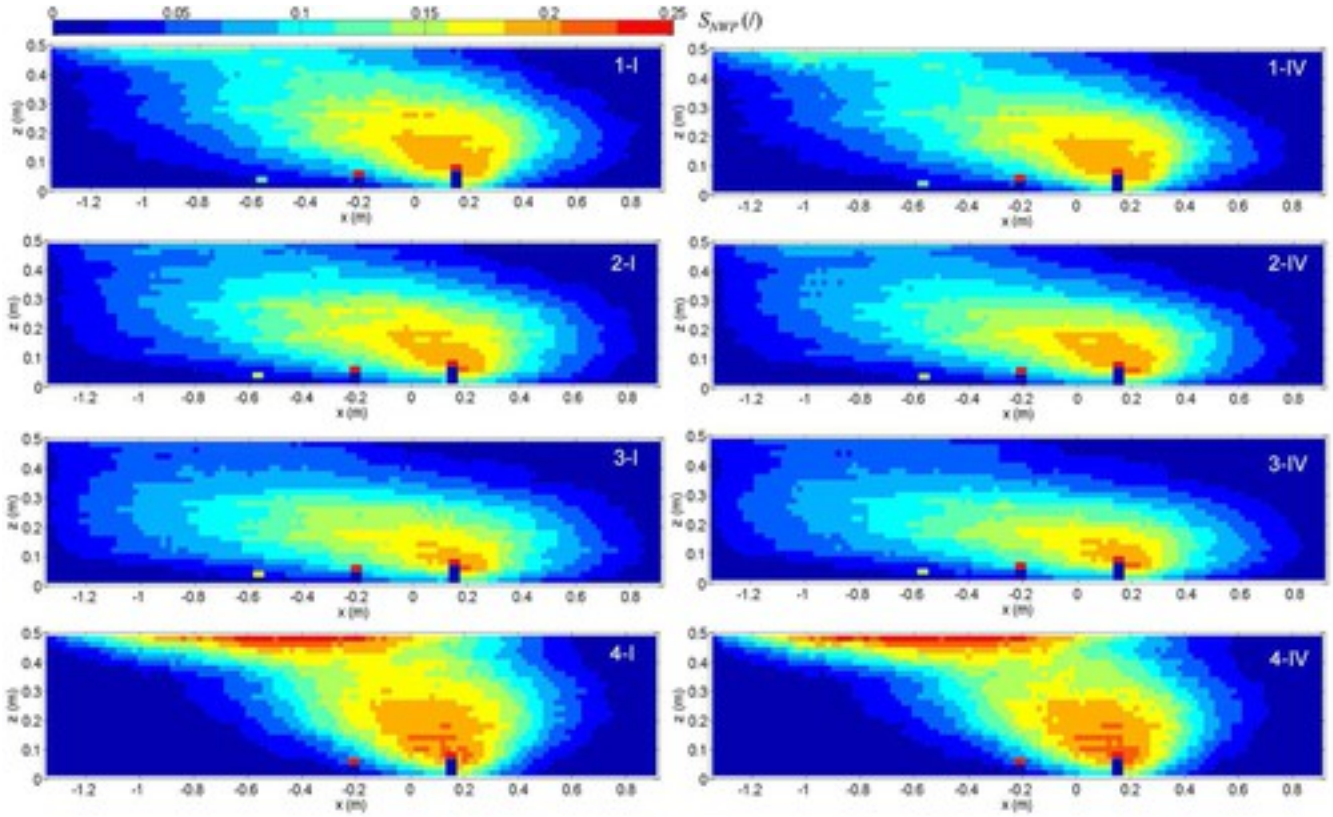

Figure 3
Open in figure viewerPowerPoint
Average value of NWP saturation at t = 100 days for simulations 1-I, 1-IV, 2-I, 2-IV, 3-I, 3-IV, 4-I, and 4-IV.
Caption

Figure 4 shows the evolution of the average NWP saturation value of simulations 2-I and 2-IV for times between 24.16 days and 70 days. At t = 24.16 days the average NWP saturation is higher for simulation 2-IV than 2-I. The post-injection period of simulation 2-IV, after 2 L are injected, at t = 24.16 days is only of 5.56 days; whereas for simulation 2-I the post-injection

period is equal to 22.24 days. Thus, the NWP has not yet redistributed in its totality and NWP saturation greater than the residual saturation value can be found for simulation 2-IV. As time increases, the influence of background flow and buoyancy forces is appreciated in the redistribution of the $scCO_2$. The content of $scCO_2$ in the tank for simulation 2-IV decreases until it reaches a similar distribution to simulation 2-I.

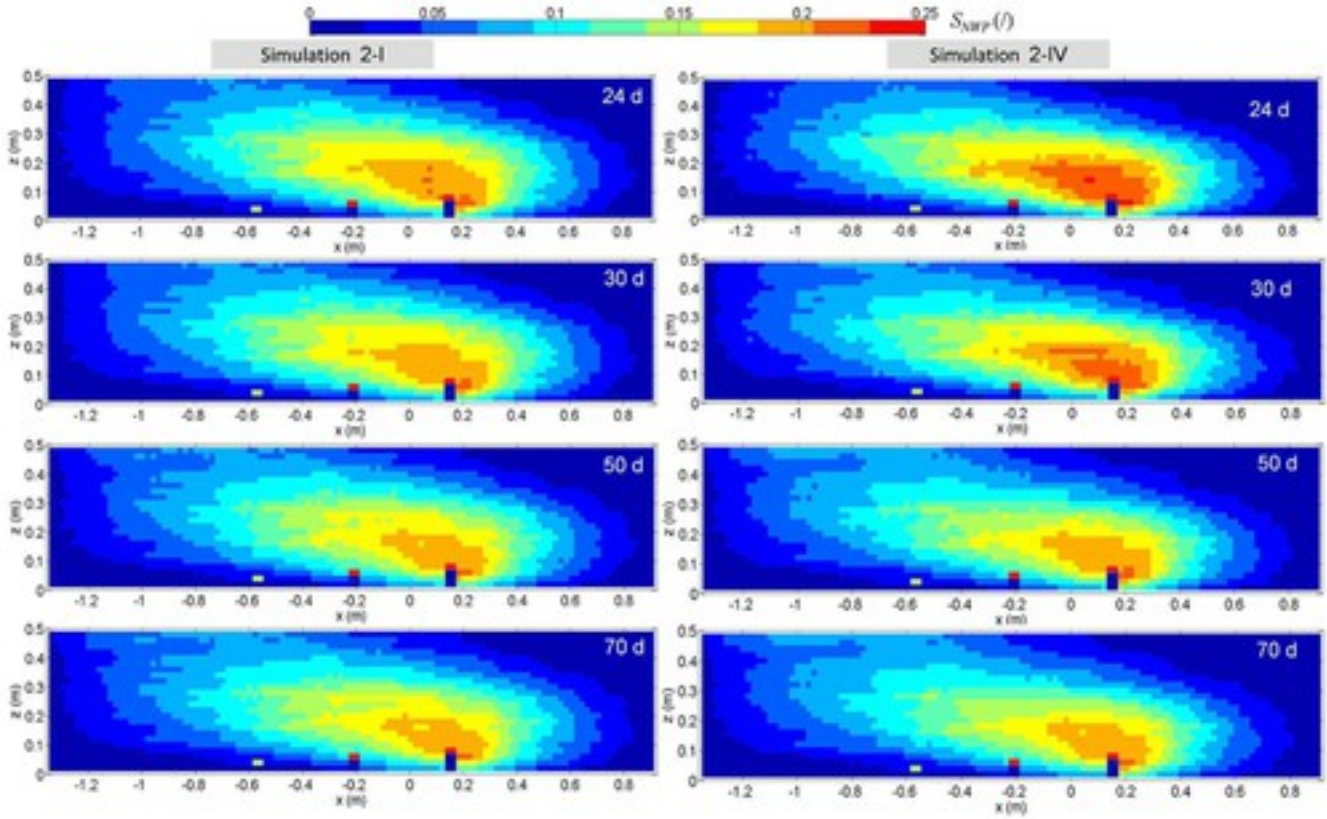

Figure 4

Open in figure viewerPowerPoint

Average value of NWP saturation for simulations 2-I (left) and 2-IV (right) for times between 24 days and 70 days.

Caption

Figure 5 displays box-plots of the center of the NWP volume in the vertical direction ($\mathbb{Z}_c$ in Eqn 8) at t = 100 days. Simulations 1, 2, and 3 show a lower distribution of the plume for injection strategy IV. For instance, simulation 1-I has a median and a first quartile value of 25.2 cm and 22.0 cm, respectively; whereas for simulation 1-IV the median is 24.7 cm and the first quartile value is 21.2 cm.

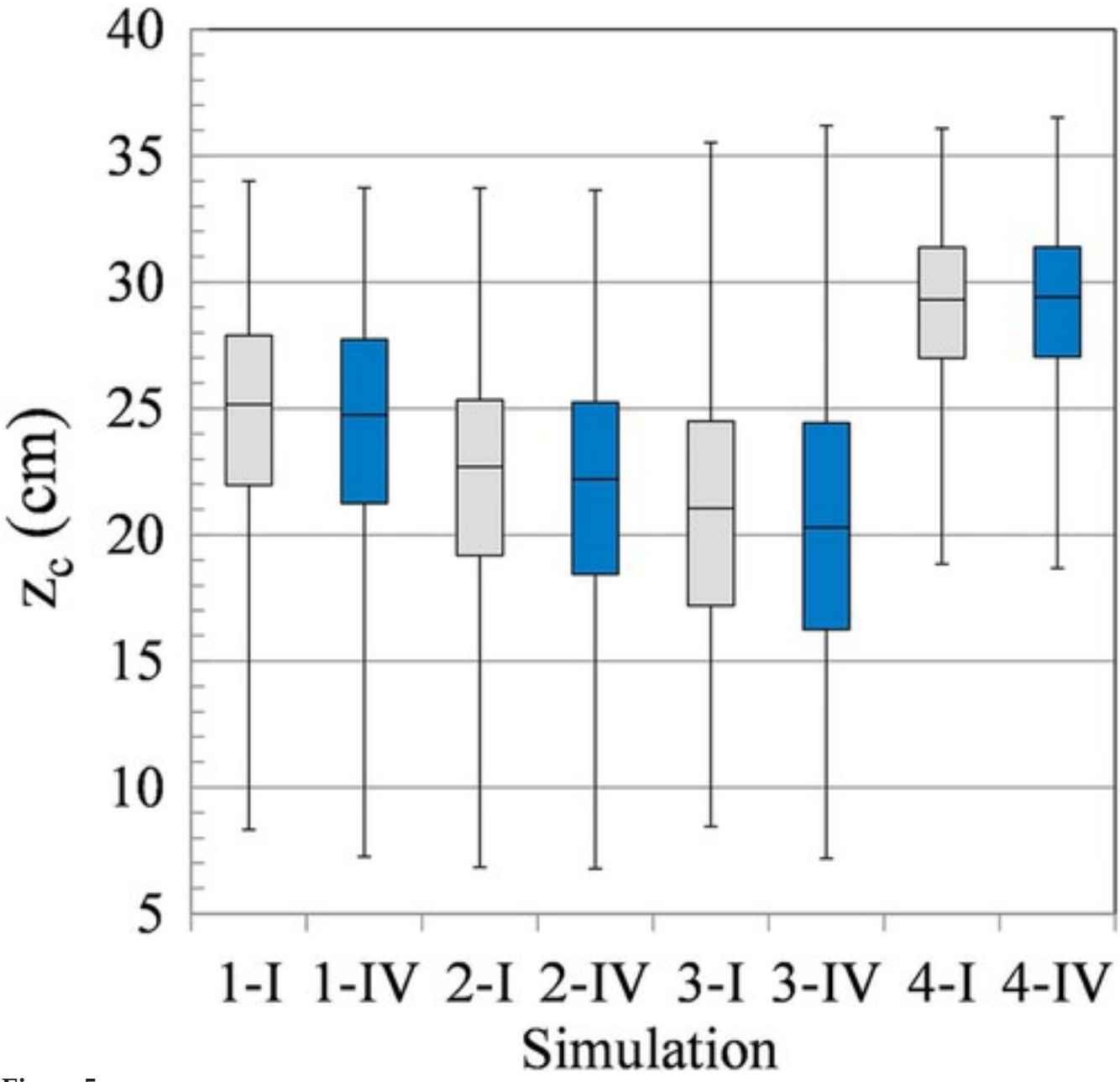

Figure 5

Open in figure viewerPowerPoint

Vertical displacement of the NWP plume center at t = 100 days. Injection strategy I is in gray and IV in blue.

Caption

The vertical migration of the NWP is affected by the heterogeneity of the formation. Simulation 4 clearly shows that the center of the NWP volume in the vertical direction is much higher than for simulations 1 to 3; however, simulations 4-I and 4-IV produce very similar results of z_c. In simulation 4 the anisotropy of permeability variance in the vertical direction is more important than in simulations 1 to 3, thus favoring the move of the plume vertically. The vertical migration

of the NWP through the heterogeneous formation not only depends on the heterogeneity, but also on the injection scheduling. The NWP migrates vertically until it finds a layer with low permeability. Then the NWP migrates horizontally through the higher permeable layer and is accumulated under the low permeable layer. If the capillary pressure exceeds the entry pressure of the low permeable formation, the NWP will penetrate it and advance through this layer. This phenomenon only occurs if enough NWP saturation accumulates under the low permeable layer. When applying more cycles, such that in injection strategy IV, the same volume of NWP is injected during more frequent but shorter injection periods. This allows repeated relaxations and redistributions of the NWP in the aquifer, thus less volume is pooled under the low permeability layer; whereas when applying injection strategy I the total volume of NWP is injected in only one injection period. Thus, more NWP is accumulated under the low permeable layer and entry pressure can be exceeded before plume redistribution starts.

Figure 6 displays results of the lateral (σ_{xx} in Eqn 9) and vertical spread (σ_{zz} in Eqn 9) of the NWP. Lateral spread of the plume (Fig. 6(a)) is rather sensitive to the injection strategy applied. Consistently injection strategy I presents a lower spread of the plume in the lateral direction. Generally, in Fig. 6(b), injection strategy I displays a lower vertical spread than injection strategy IV. Note that in Fig. 6 the 75th of the cases for injection strategy I produce a lower lateral and vertical spreads than injection strategy IV, indicating a more compressed distribution of the NWP. However, simulation 3 presents a higher vertical spread for injection strategy I than for injection strategy IV.

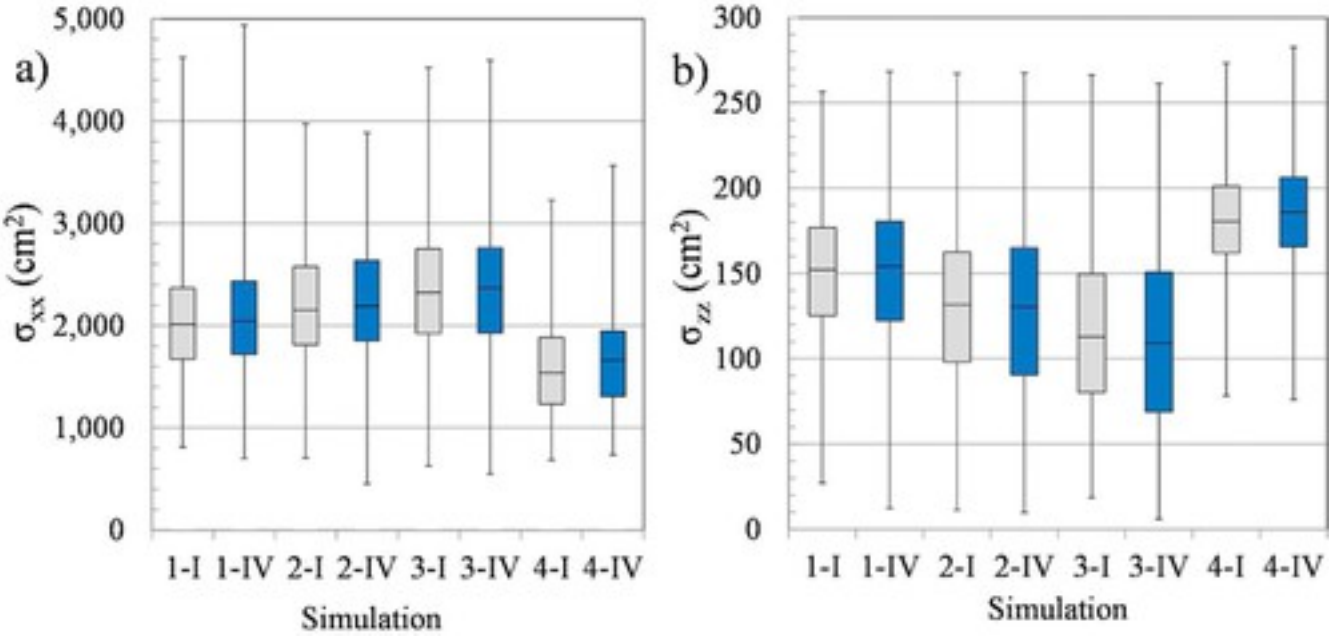

Figure 6

Open in figure viewerPowerPoint

(a) Lateral and (b) Vertical spread of the plume for simulations 1 to 4. Injection strategy I is in gray and IV in blue.

Caption

The injection strategy also affects the distribution of the NWP within the sands. Figure 7displays the NWP volume distribution in each type of sand for simulations 2 (simulations 1, 3, and 4 are not shown here). Both injection strategies I and IV show similar distribution of the NWP within the sands: larger volumes of NWP are stored in sands with larger presence (refer to Fig. 2 for histograms of sands) in the aquifer. In general, injection strategy I can store more NWP, displaying a higher volume of NWP especially within low permeable areas ($\ln k$ = -24.96 and $\ln k$ = -24.11) than injection strategy IV. As previously mentioned, the entry pressure of low permeable layers can be exceeded more easily by applying an injection strategy with only one cycle.

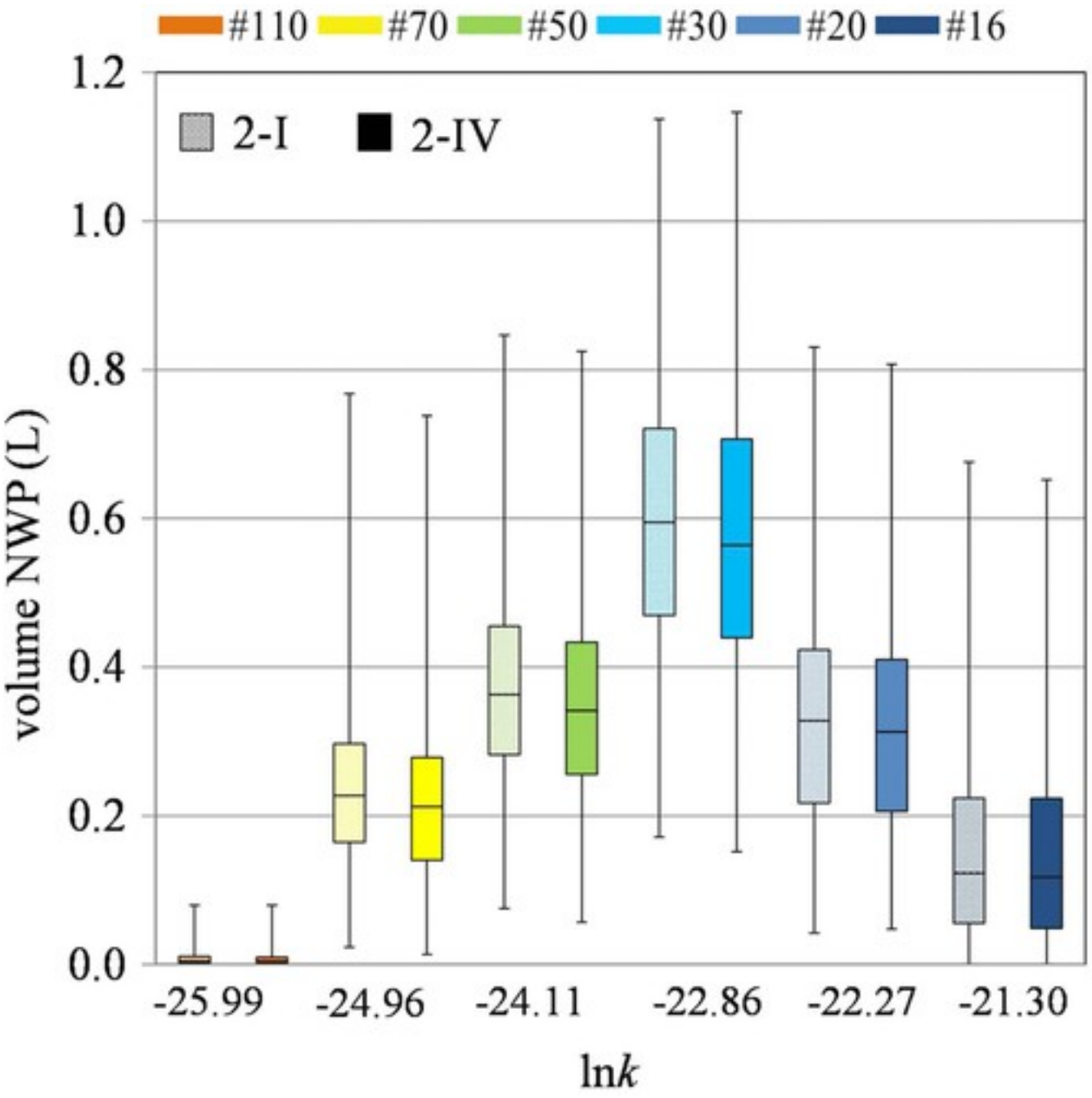

Figure 7

Open in figure viewerPowerPoint

Non-wetting phase distribution stored at each sand for simulation 2.

Caption

To further investigate the influence of the injection strategy, three new injection strategies are designed for simulation 2 to compare with injection strategy I (which has a time of injection equal to 1.92 days). These three injection strategies, named A to C, present higher injection rates than injection strategy I (Table 2). Injection strategy A, at t = 1.92 days, has injected the total

volume of 2 L with an injection rate of 1.33 L/d including one time interval of 0.42 days between the two injection phases (injection cycle + relaxation time + injection cycle). Injection strategy B is similar to A; however, the injection rate is 2 L/d and the time interval between injection cycles is 0.9 days. Injection strategy C injects the total volume of NWP with an injection rate of 1.33 L/d uninterruptedly (only one injection cycle) finishing the injection period at t = 1.5 days. Table 8 includes results of the number of successful realizations in which $scCO_2$plume is trapped in its totality (2 L) in the secure zone and the leakage of $scCO_2$ from the secure zone at t = 100 days.

Table 8. Results for simulations 2-I, 2-A, 2-B, and 2-C at t = 100 days.

Injection strategy	**2-I**	**2-A**	**2-B**	**2-C**
Successful realizations*	88	90	99	100
Leakage $scCO_2$ %	13.6	13.2	12.0	12.4

- *Number of realizations in which $scCO_2$ plume is trapped in its totality (2 L) in the secure zone at t = 100 days

Injection strategy 2-C (with the highest injection rate) produces more successful realizations that store the totality of the NWP in the secure zone; however, it is only greater than 2-B by one realization. Nevertheless, injection strategy 2-B shows less leakage of NWP from the secure zone indicating that a relaxation time between injection periods can enhance the capillary trapping of the NWP. Figure 8 compares the cumulative distribution function of the NWP volume trapped in the secure zone at time 100 days for simulations 2-I, 2-IV, and 2-B. In this figure injection strategy B shows larger NWP volumes trapped in the secure zone for 100% of the ensemble realizations. According to Fig. 8, predominantly an injection strategy with less cycles and higher injection rate, such as 2-B, enhances capillary trapping of NWP, since higher pressure buildup associated with higher injection rates can exceed more easily the entry pressure of low permeable areas, effectively trapping more $scCO_2$ in the reservoir.

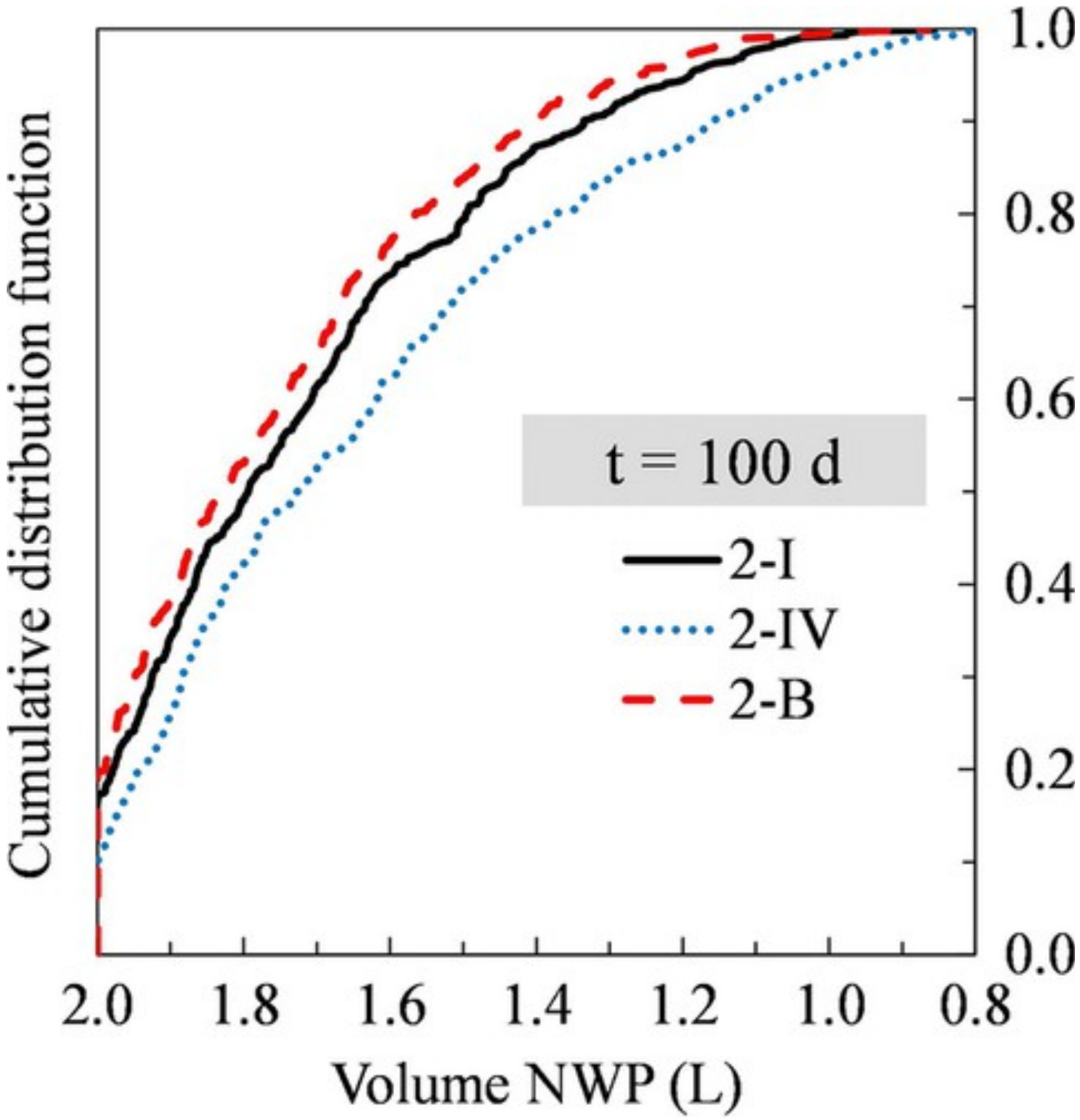

Figure 8

Open in figure viewerPowerPoint

Cumulative distribution function of the NWP volume trapped in the secure zone at time 100 days for simulations 2-I, 2-IV, and 2-B.

Caption

Although results indicate that the NWP stored in the tank and the plume-scale effective trapping saturation can be increased by applying an injection strategy with fewer cycles, we point out that this result is only valid for the specific geological setup considered here and considering the assumptions behind the numerical model (e.g. hysteresis is neglected). Moreover, the total

leakage of $scCO_2$ (Table 7) is only slightly greater for injection strategy IV than strategy I for simulations 1 to 4. However, our study is based on a limited range of geological structures based on long horizontal and short vertical correlation lengths and for intermediate-scale tank experiments. Interestingly, Herring *et al*.14 showed that multiple cyclic injection schemes applied to a pore-scale experiments enhance the residual trapping of $scCO_2$; the increased residual trapping of their experiments is attributed to a hysteretic effect. Therefore, sensitivity analyses on the effect of injection strategy to enhance capillary trapping need to be done for broader ranges of geological configurations and scales, different from this study.

Summary and conclusions

In this study, we performed a stochastic analysis to investigate how to enhance capillary trapping by designing intermittent injection strategies. The stochastic analysis was implemented to different permeability fields based on laboratory experiments at the intermediate scale. The heterogeneous permeability fields were created using different variances of the ln$k$ probability distribution function and different horizontal correlation lengths. Six types of sands with their corresponding relative permeability curves, and parameters of the primary drainage were used to characterize the heterogeneous formation. We applied several sequential injection schemes that alternate injection and relaxation periods to place the same volume of NWP. Results indicate that distribution of the NWP through the storage formation depends on the injection strategy implemented. In general, for the geological setup of this study and based on the assumptions behind the model, we observed that injection schemes including less alternated phases of injection and non-injection and higher injection rates increase slightly the volume of $scCO_2$ capillary trapped in the secure zone of the reservoir. Injection strategies with fewer cycles of injection pulse and relaxation show a higher distribution of the NWP plume. Fewer cycles allow a greater accumulation of the NWP under areas of low permeability, which helps to exceed their entry pressure and redistribute vertically and more efficiently through the reservoir.

These findings suggest that by using information on the heterogeneity, time-phased $scCO_2$injection schemes can be developed to enhance capillary trapping and secure permanence by confining the trapping zones to safe zones of the formation and minimizing possible leakages. Future research needs to include the influence of hysteresis and the study of field-site scales, since fluid displacement governed by capillary forces, such as $scCO_2$-brine flow presented here, can be affected by hysteresis and heterogeneity.

Acknowledgements

Funding for this research is provided by the U.S. Department of Energy through the National Energy Technology Laboratory's CO2 sequestration R&D Program under grant DE-FE0004630 and National Science Foundation Award no.: EAR-1045282 through the Hydrologic Sciences Program.

Biographies

- 

  Ana González-Nicolás Ana González-Nicolás is a scientific engineer associate in Energy Geosciences Division at Lawrence Berkeley National Laboratory. Her research interests include multiphase flow, transport phenomena in porous media, geostatistical analysis, and optimization methods. She earned her Ph.D. in Civil Engineering at Colorado State University.

- 

  Luca Trevisan Luca Trevisan is a postdoctoral fellow at the Gulf Coast Carbon Center of the Bureau of Economic Geology, the University of Texas at Austin. His current research addresses the influence of geologic heterogeneity at cm-to-m scale on subsurface fluid flow of carbon dioxide using continuum-based and invasion percolation models. He obtained his Ph.D. in Environmental Science and Engineering from Colorado School of Mines.

- 

  Tissa Illangasekare Tissa Illangasekare is the AMAX Distinguished Chair at CSM. He is a Fellow of AGU, AAAS,ASCE and SSSA. Recipient EGU's Darcy Medal, AGU's Langbein Lecture Award and 7th Prince Sultan Bin Abdulaziz International Groundwater Prize. He was past editor of *Water Resources Research*. His research is in numerical and physical modeling of porous media processes.

- 

  Abdullah Cihan Abdullah Cihan is a geological scientist in Energy Geosciences Division at Lawrence Berkeley National Laboratory. His general research area involves theoretical understanding and modeling of multiphase flow and transport phenomena across scales of subsurface systems. His research applications have been related to geologic carbon sequestration, gas/oil production from unconventional reservoirs, reservoir management, evaporation from soil, and groundwater remediation.

- 

  Jens Birkholzer Jens Birkholzer is a senior scientist at the Lawrence Berkeley National Laboratory. He currently serves as the Director for the Energy Geosciences Division (EGD) in the Earth and Environmental Systems Area (EESA). His scientific emphasis centers on

understanding and modeling coupled multi-phase fluid, gas, solute and heat transport in complex subsurface systems such as or fractured rock or heterogeneous sediments.